Inferred Increases in the Convective Entrainment Rate under Climate Change: Implications for Tropical Temperature Trends

Simchan Yook[1]* and David W. J. Thompson[2,3]

Affiliations:

[1] Department of Earth, Atmospheric, & Planetary Sciences, Massachusetts Institute of Technology, Cambridge, MA, USA.

[2] Department of Atmospheric Science, Colorado State University, Fort Collins, CO, USA.

[3] Centre for Ocean and Atmospheric Sciences, School of Environmental Sciences, University of East Anglia, Norwich, UK.

* Corresponding author. Email: syook@mit.edu

Abstract:

Tropical-mean tropospheric temperatures are lower than those predicted by the moist adiabatic lapse rate. The differences ΔT between tropical-mean temperatures and a moist adiabat increase notably in climate change simulations, with implications for trends in CAPE and tropical temperatures. The increases in ΔT under climate change have been interpreted as a consequence of a fixed convective entrainment rate acting on increases in the saturation deficit between undilute convecting plumes and the environment. Here we use a zero-buoyancy entraining plume model to argue that the increases in ΔT found in climate change simulations can *only* be reproduced when the entrainment rate also increases substantially with temperature. The relationship between temperature and the entrainment rate implied by the plume model is roughly linear and is reproducible when the model is constrained by observations. The implied increases in the entrainment rate with global warming have implications for long-term changes in both the mean and variance of tropical temperatures.

1. Introduction

The vertical profile of tropical-mean tropospheric temperatures T is strongly constrained by the physics of the moist adiabatic lapse rate. To zero-order, temperatures in convecting regions closely follow a moist adiabat since the air is saturated, and temperatures in convecting regions are rapidly communicated to clear-sky regions through atmospheric dynamical processes (Charney 1963; Stone and Carlson, 1979; Sobel and Bretherton 2000). However, T also exhibits well-known departures from those predicted by the moist adiabat.

The differences between tropical-mean temperatures and a moist adiabat (ΔT) are robust in the *climatological-mean*. Tropical-mean temperatures are several degrees lower than those predicted by a moist adiabat in both observations (Singh and O'Gorman 2013; Keil et al., 2019) and control simulations run on fully coupled Earth System Models (ESMs; Po-Chedley et al. 2019; Keil et al., 2019; Miyawaki et al. 2020). Importantly, the differences ΔT are also expected to increase under *climate change*. Numerical simulations forced with increasing greenhouse gases widely indicate robust increases in ΔT in response to rising temperatures (Santer et al. 2005; Sobel and Camargo 2011; Fasullo 2012; Zhou and Xie, 2019; Miyawaki et al. 2020; Bao and Stevens 2021; Bao et al. 2021). The simulated increases in ΔT are associated with notable

increases in convective available potential energy (CAPE) (Romps 2011; Muller et al. 2011; Singh and O'Gorman 2013; Seeley and Romps, 2015), with implications for increases in lightning strikes (Romps et al., 2014), the strength of convective updrafts (Singh and O'Gorman 2013), and climate sensitivity (Bao and Stevens 2021). The detection of observed trends in upper tropical tropospheric temperatures - and thus tropical ΔT - is complicated by, for example, the influence of stratospheric layers on remotely sensed retrievals of upper tropospheric temperatures and biases in radiosonde measurements (e.g., Santer et al., 2005, 2017; Flannaghan et al., 2014; Steiner et al., 2020). Nevertheless, analyses of ERA-40 (e.g., Riemann-Campe et al., 2009), radiosonde data over the tropics (e.g., Gettelman et al. 2002; Santer et al. 2005), radiosonde data over NH midlatitudes (Chen and Dai 2023), and both radiosonde and microwave sounding products over the tropics (e.g., Steiner et al., 2020; c.f., Fig. 13) generally suggest changes in tropical temperatures that are indicative of increases in ΔT or increases in CAPE.

Why does ΔT - and thus CAPE - increase under global warming? In the climatology, the depression of tropical temperatures relative to a moist adiabat is thought to arise from the mixing of relatively dry environmental air into convecting plumes through entrainment. The importance of convective entrainment can, in turn, be decomposed into two factors: a) the entrainment rate ε, which reflects the amplitude of turbulent mixing and also the distribution of convective plumes across the tropics; and b) the differences in moist static energy Δh between convecting plumes and the surrounding environment. The changes in ΔT under climate change are thought to arise primarily from increases in Δh, since the differences in moist static energy between plumes and the surrounding environment scale with the saturation vapor pressure of the air (Singh and O'Gorman 2013). Here we argue that the changes in ΔT found in climate change simulations are only partially accounted for by changes in Δh, and are also indicative of substantial increases in the entrainment rate ε.

The paper is organized as follows. Section 2 outlines the data sources and analysis technique. Section 3 confirms that tropical-mean tropospheric temperatures T are less than those predicted by the moist adiabat in both observations and climate simulations, and that ΔT increases notably with temperature. In Section 4, we demonstrate using the zero-buoyancy plume model of Singh and O'Gorman (2013) that the variations in ΔT found in both climate change simulations and observations are underestimated by the attendant changes in Δh, and are only reproducible if the entrainment rate is assumed to increase roughly linearly with atmospheric

temperature. In Section 5 we argue that the near-linear relationship between temperature and the entrainment rate has substantial implications for long-term changes in both the mean and variance of tropical temperatures. Conclusions are provided in Section 6.

2. Data and analysis

The primary climate model results are derived from the 40 member large-ensemble of simulations run on the National Center of Atmospheric Research (NCAR) Community Earth System Model version 1 over the period 1950-2100 (NCAR CESM1; Hurrell et al. 2013, Kay et al. 2015). The output is publicly available via the NCAR Multi-Model Large Ensemble Archive (MMLEA; Deser et al., 2020) and archived on resources sponsored by the US Climate and Ocean Variability, Predictability and Change (CLIVAR) Working Group on Large Ensembles and National Science Foundation/Computational and Information Systems Laboratory/Yellowstone. The experiments are integrated with Coupled Model Intercomparison Project Phase 5 (CMIP5) historical forcing from 1920 to 2005 and Representative Concentration Pathways 8.5 (RCP8.5) forcing over the period 2006-2100. Key numerical results are reproduced using output from large-ensembles run on three other Earth system models: The Commonwealth Scientific and Industrial Research Organisation Mk3.6 (30 simulations; Jeffrey et al., 2013), the Canadian Centre for Climate Modeling and Analysis CanESM2 (50 simulations; Kirchmeier-Young et al. 2017), and the Geophysical Fluid Dynamics Laboratory ESM2M (30 simulations; Rodgers et al. 2015). All results are based on annual-mean output.

Observational results are based on reanalysis data from the European Center for Medium-Range Weather Forecasts Re-Analysis 5 (ERA5; Hersbach et al., 2020). Key observational findings are reproduced using radiosonde data from the Integrated Global Radiosonde Archive Version 2 (IGRA2; Durre et al., 2018).

Throughout the analyses we use the following definitions:

- *T(z)* refers to tropical-mean temperatures averaged over the latitude band 20°S-20°N.

- $T_{MLR}(z)$ refers to the vertical profile of temperatures that results from integrating *T* at 700 hPa vertically following the moist lapse rate. The moist adiabatic lapse rate is found as

123 $$\Gamma_m = \Gamma_d \frac{1 + \frac{L_v w^*}{R_d T}}{1 + \frac{{L_v}^2 w^*}{c_p R_v T^2}}$$

124

125 where c_p is the specific heat capacity at constant pressure, L_v is the latent heat of vaporization,
126 w^* is the saturation mixing ratio, * denotes the saturation value, R_d and R_v are the gas constants
127 for the dry air and water vapor, $\Gamma_d = \frac{c_p}{g}$ is the dry adiabatic lapse rate, and g is the gravitational
128 acceleration. The sensitivity of the results to the use of the 700hPa level as a starting point for the
129 integration is discussed further below.

130 - $\Delta T(z)$ is defined as the difference between T and T_{MLR}, that is $\Delta T = T - T_{MLR}$.
131 Negative values of ΔT indicate that simulated or observed tropical-mean temperatures are lower
132 than that predicted by the moist lapse rate, and vice versa. Note that by construction $\Delta T = 0$ at
133 700 hPa.

134

135

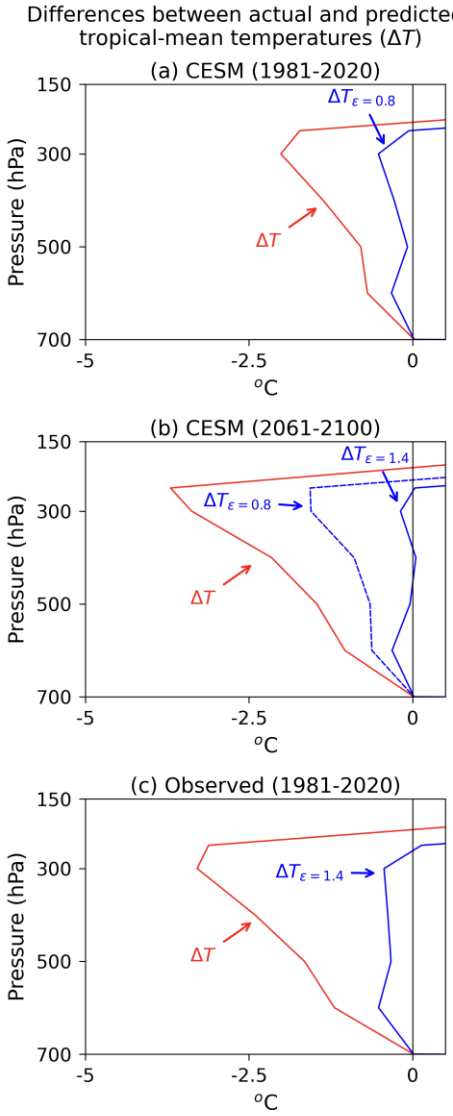

Figure 1. Differences ΔT between actual tropical-mean temperatures and those predicted by the plume model. Results are based on CESM1 output over 1981-2020 (left); CESM1 output over 2061-2100 (middle); and ERA5 data over 1981-2020 (right). The predicted temperatures are based on the zero-buoyancy entraining plume model where the entrainment parameter is set to $\epsilon = 0$ (red lines; note that $\epsilon = 0$ corresponds to the moist lapse rate and the differences are labeled as ΔT); $\epsilon = 0.8$ (blue line in left), $\epsilon = 0.8$ (dashed line in middle), and $\epsilon = 1.4$ (solid lines in middle and right panels). The zero-buoyancy model profiles are integrated from the 700 hPa level. The zero line indicates where actual and predicted temperatures are identical.

3. Increased Differences Between Tropical Temperatures and the Moist Adiabat Under Global Warming

The red lines in Figures 1a and 1b show ensemble-mean values of ΔT from the NCAR CESM1 averaged over two time periods: 1981-2020 (Fig. 1a) and 2061-2100 (Fig. 1b). The red line in Fig. 1c shows the corresponding results based on ERA5 averaged over the 1981-2020

period. As noted extensively in previous research (e.g., Singh and O'Gorman, 2013; Keil et al., 2019; Zhou and Xie 2019; Miyawaki et al., 2020; Bao and Stevens 2021), tropical-mean temperatures exhibit marked departures from those predicted by the moist lapse rate. The departures are notably larger during the latter period of the simulation: Upper tropospheric temperatures are about *~1.5 – 2K* less than those predicted by the moist lapse rate in the current climate (Fig. 1a) but *~3 - 3.5K* less in the latter half of the 21st century (Fig. 1b). Interestingly, the ERA5 values of ΔT (Fig. 1c) are roughly twice as large as those found in the CESM simulation averaged over the 1981-2020 period but bear close resemblance to those found from CESM output averaged over the latter part of the 21st century.

The systematic nature of the relationship between ΔT and lower tropospheric temperature is readily apparent when the results are discretized by year. Figure 2a shows annual-mean values of ΔT derived from all 40 CESM simulations over the period 1950-2100, where each line denotes ΔT for an individual year, and the colors of the lines indicate the corresponding 700hPa temperature used as a starting point for the vertical integration of the moist lapse rate. Figure 2d shows analogous results based on ERA5 for all years 1980-2020. From Fig. 2a it is clear that ΔT increases systematically with tropical-mean temperature, increasing from $\Delta T = -1.5K$ at 300hPa for 700hPa temperatures around 280K (output from the mid 20th century) to $\Delta T = -4.5K$ at 300hPa for 700hPa temperatures around 286K (output from the late 21st century). The same relationship between temperature and ΔT is also found in association with annual-mean ERA5 data over 1980-2020 (Fig. 2d). As noted above, the ERA5 values of ΔT bear closest resemblance to simulated values from the latter part of the 21st century (i.e., the warmest profiles in Fig. 2a).

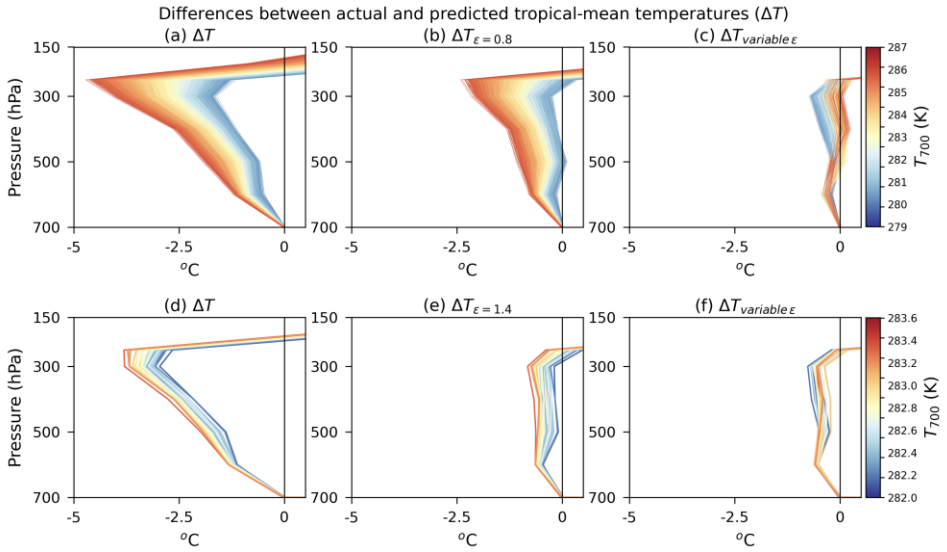

Figure 2. (a) Differences ΔT between actual tropical-mean temperatures and those predicted by the plume model, where the predicted temperatures are based on the zero-buoyancy entraining plume model where the entrainment parameter is set to $\epsilon = 0$. The differences ΔT are plotted separately for each year from 1950 to 2100 in all 40 simulations, where the color of each line indicates the corresponding annual mean 700 hPa temperature. (b) As in panel (a), but the predicted temperatures are based on the zero-buoyancy entraining plume model where the entrainment parameter is set to $\epsilon = 0.8$ during all years (c) As in panel (b), but the predicted temperatures are based on the zero-buoyancy entraining plume model where the entrainment parameter varies as per the linear fit of the grey dots in Fig. 3a (given in Eq. 4b). (d-f) As in panels (a)-(c), but for results based on ERA5 output over the 1981-2020 period. The entrainment rate for panel (e) is set to $\epsilon = 1.4$, and the linear fit is given by the linear fit of the black dots in Fig. 3a (given in Eq. 4a)

4. Implied increases in the convective entrainment rate

Why does ΔT increase as lower tropospheric temperatures increase? As discussed in the Introduction, the climatological-mean values of ΔT are thought to arise from a variety of factors, including the entrainment of dry air into regions of deep convection, the signature of convective plumes with different vertical extents and entrainment rates in tropical-mean temperatures, and the effects of the large-scale circulation on the thermal stratification of the atmosphere (Romps and Kuang 2010; Singh and O'Gorman 2013; Zhou and Xie 2019; Keil et al., 2019; Miyawaki et al. 2020; Bao and Stevens, 2021; Bao et al. 2021). The increases in ΔT under climate change have been linked primarily to increases in the differences in moist static energy Δh between plumes and the surrounding environment, since such differences scale with the saturation vapor deficit of the environment (Singh and O'Gorman 2013; Seeley and Romps 2015).

Here we revisit the processes that drive changes in ΔT under climate change using the zero-buoyancy plume model developed in Singh and O'Gorman (2013). Briefly, the model is

derived as follows. The vertical structure of moist static energy (MSE) in an entraining plume can be approximated as

$$\frac{dh}{dz} = -\varepsilon \Delta h \quad (1)$$

where ε is the entrainment rate, $\Delta h = h - h_e$ denotes the difference in MSE between the plume and the environment, $h = c_p T + gz + L_v q$ is the MSE, q is the specific humidity, and the subscript *e* denotes the environment. The zero-buoyancy plume model is motivated by the observation that the buoyancies of convecting clouds in the tropical atmosphere are relatively small such that at a given level $T \sim T_e$ (Lawson, 1990; Wei et al., 1998; Sherwood et al., 2013; Singh and O'Gorman 2013; Romps and Charn, 2015). In this case, the differences in MSE between an undilute plume and the environment reduce to $h - h_e = L_v(q - q_e)$, and the MSE and specific humidity of the plume are equal to those for the environment at saturation such that $h = h_e^*$ and $q = q_e^*$. Substituting the above into (1) yields an expression for the vertical profile of environmental MSE that arises from the effects of convective entrainment:

$$\frac{dh_e^*}{dz} = -\varepsilon L_v q_e^* (1 - RH) \quad (2)$$

where $RH \sim \frac{q_e}{q_e^*}$ is the relative humidity of the environment (Singh and O'Gorman 2013; Seeley and Romps 2015). The differences in MSE between an environment influenced by convective entrainment (Eq. 2) and one in which the convecting plumes are not diluted ($\frac{dh_u}{dz} = 0$, where the subscript *u* denotes an undilute plume) can be found by integrating Eq. 2 vertically from cloud base. The results of the integration can then be combined with the Clausius-Clapeyron relation to yield an expression for the temperature of an environment influenced by convective entrainment T_ε as (i.e., Singh and O'Gorman 2013 Eq. 4):

$$T_\varepsilon = T_{MLR} + \frac{1}{L_v \frac{\partial q^*}{\partial T} + c_p} \int_{z_b}^{z} \varepsilon' L_v (1 - RH) q_e^* \, dz \quad (3)$$

where z_b is cloud base, T_{MLR} is the moist adiabat integrated vertically from z_b, and T_ε is the temperature of the entraining plume. Following Singh and O'Gorman (2013), the entrainment profile is approximated as $\varepsilon'(z) = \frac{\varepsilon}{z}$ for $z \geq z_b$ and $\varepsilon'(z) = 0$ for $z < z_b$, where ε is specified and ε' decreases linearly with height to account for the fact that clouds at different locations detrain at different levels. The key is that Eq. (3) provides a theoretical estimate of tropical temperatures as a function of the relative humidity of the environment and a specified entrainment rate. Following our definition for $\Delta T = T - T_{MLR}$, we define the differences between tropical-mean temperatures and those predicted by the entraining zero-buoyancy plume model for a given entrainment rate as $\Delta T_\varepsilon = T - T_\varepsilon$.

The solid blue lines in Figs. 1a-c show ΔT_ε derived from Eq. 3, where the entrainment rate ε is determined empirically to minimize ΔT_ε at the 250hPa level. We fit T_ε to T at 250 hPa since 1) the differences between T and the moist adiabat peak near this level (Figs. 2a, d); and 2) the moist adiabat is less relevant for understanding the temperature profile above ~250hPa (Folkins 2002, Keil et al, 2019). As done for T_{MLR}, T_ε is found by starting the integration at 700 hPa. The relative humidity is assumed fixed at 80%, since it remains roughly invariant to temperature in both models and observations (e.g, Soden et al., 2002, 2005; Soden and Held 2006). The effects of changing the relative humidity are discussed below.

The entrainment rate that provides the best fit between 250hPa temperatures and those given by the plume model differ notably between the two simulation periods (panels a and b). The best fit to CESM temperatures during the 1981-2020 period arises when $\varepsilon = 0.8$ (solid blue line in Fig. 1a), whereas $\varepsilon = 0.8$ notably overestimates tropical-mean temperatures during the 2061-2100 era (dashed blue line in Fig. 1b). Rather, the best fit to CESM temperatures during the 2061-2100 era arises when $\varepsilon = 1.4$, roughly 75% larger than the historical value. The best fit to the observations is found using an entrainment rate similar to that inferred from the CESM output over the latter period (Fig. 1c).

As discussed earlier, ΔT and ΔT_ε increase with temperature even if the entrainment rate is fixed in the case of the latter. That is because the saturation deficit Δh between an undilute parcel and the environment follows Clausius-Clapeyron scaling. This effect is captured in Eq. 3 by changes in $\frac{\partial q^*}{\partial T}$ with temperature (Seeley and Romps 2015). However, from Figs. 1a and 1b, it is

clear that fixing the entrainment rate at its 1981-2020 value ($\varepsilon = 0.8$) leads to a notable overestimate of temperatures (as indicated by negative ΔT_ε) during the 2061-2100 period.

The robustness of the relationships indicated in Fig. 1 are further evidenced in the middle column of Fig. 2. Fig. 2b shows the differences between tropical temperatures and those predicted by Eq. 3 with a fixed entrainment rate $\varepsilon = 0.8$, that is, it shows $\Delta T_{\varepsilon=0.8} = T - T_{\varepsilon=0.8}$. As in Fig. 2a, results are derived for annual-mean T profiles over 1950-2100 from all 40 CESM simulations, and colors indicate the attendant 700hPa temperatures. If increases in the saturation vapor deficit accounted for all of the increases in ΔT with climate change, then $\Delta T_{\varepsilon=0.8}$ should remain close to zero even as temperatures warm. However, as also indicated in Fig. 1b, it is clear that fixing the entrainment rate to its 1981-2020 value leads to an increasingly large overestimate of tropospheric temperature trends (increasingly negative ΔT_ε) by the plume model. Similarly, as indicated for ERA5 in Fig. 2e, fixing the entrainment rate at $\varepsilon = 1.4$ provides a close fit to the coldest ERA5 temperature profiles but again overestimates free tropospheric temperatures during warm years.

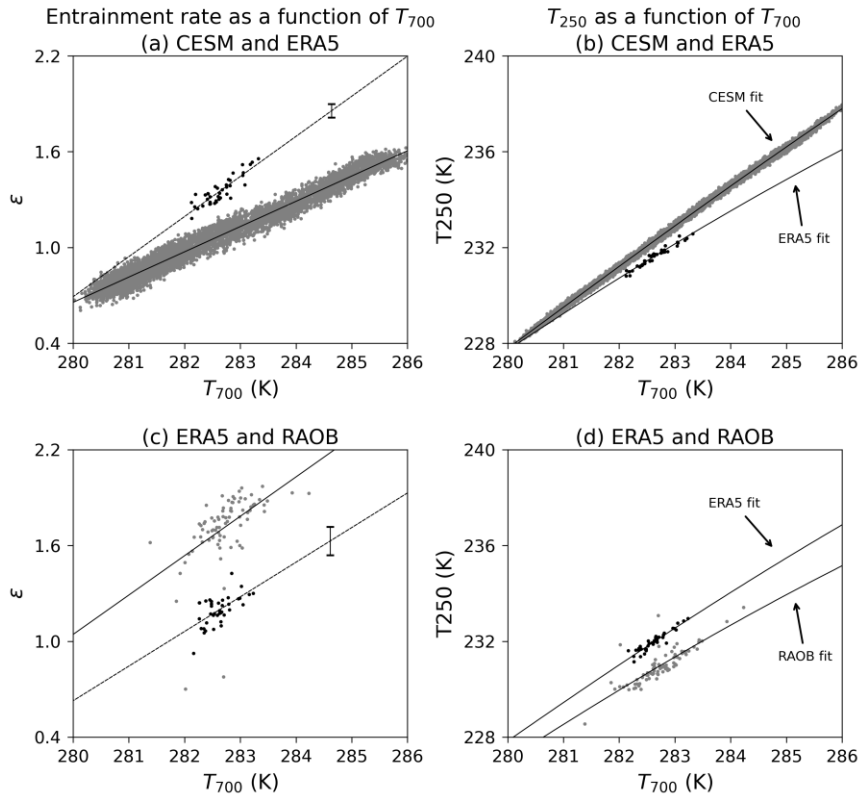

Figure 3. Top panels: (a) Scatter plot illustrating the relationship between tropical-mean temperatures at 700hPa and the entrainment rate that provides the best fit between actual and theoretical tropical-mean temperatures at 250hPa. Grey dots represents individual years from the GCM output; black dots individual years from ERA5. The black lines indicates the best fits to the model and ERA5 output and are $\epsilon = 0.25T_{700} - 70$ for ERA5 and, $\epsilon = 0.16T_{700} - 44$ for CESM. The error bar for the ERA5 data indicates the 95% confidence range, derived from the standard error of the regression. (b) Dots indicate the scatter plots of actual tropical-mean temperatures at 700 hPa and 250 hPa from CESM1 output (grey dots) and ERA5 (black dots). Lines indicate the predicted relationships using the plume model where the entrainment rate varies with 700hPa temperature as per the linear fits in panel (a). Bottom panels: (c) Black dots and linear fit: As in the ERA5 results from panel (a), but ERA5 data are sampled at locations where RAOB output are available. Grey dots: Results based on tropical-mean temperatures from radiosonde data. (d) Black dots and linear fit: As in panel (b), but ERA5 data are sampled at locations where RAOB output are available and the expression for the entrainment rate is given by the black fit in panel (c). Grey dots and linear fit: Results based on tropical-mean temperatures from radiosonde data and the expression for the entrainment rate is given by the grey fit in panel (c).

Figure 3 explores in more detail the relationships between T and the entrainment rate. The grey dots in Fig. 3a show the entrainment rate required to minimize ΔT_ε at 250hPa, where each dot shows results for one year of annual-mean output from the 40 CESM1 simulations, and the x-axis indicates the corresponding 700 hPa temperature that is used as a basis of the integration in Eq. 3. Note that there are 6040 dots derived from 40 ensemble members and 151 years/simulation. The black dots in Fig. 3a show the same results for annual-mean ERA5 data. The solid lines show the linear least squares best fits between T_{700} and ε, and are equal to

(4a) $\varepsilon_{ERA5} = (0.25 \pm 0.02)K^{-1} \times T_{700} - 70$

and

(4b) $\varepsilon_{CESM} = (0.16 \pm 0.00)K^{-1} \times T_{700} - 44.$

where the range denotes the 95% confidence range derived from the standard error of the regression. From Fig. 3a, it is clear that both CESM and ERA5 indicate robust linear relationships between a) cloud base temperatures (i.e., assumed 700hPa in Fig. 3a) and b) the entrainment rate required by the plume model to simulate 250hPa temperatures. Notably, the amplitude of $\frac{\Delta\varepsilon}{\Delta T_{700}}$ is roughly 50% larger in observations than it is in CESM.

The linear relationship between T_{700} and ε rate found in ERA5 data is reproducible in results based on radiosonde data. The grey dots in Fig. 3c show results analogous to those

indicated in Fig. 3a, but for tropical-mean temperatures from the IGRA radiosonde data. The black dots in Fig. 3c are a reproduction of the ERA5 results from Fig. 3a, but in this case the ERA5 data are sampled at locations where RAOB output are available. The best fits to the results in Fig. 3c are found as:

(4c) $\varepsilon_{RAOB} = (0.25 \pm 0.05)K^{-1} \times T_{700} - 68$

and

(4d) $\varepsilon_{ERA5} = (0.22 \pm 0.05)K^{-1} \times T_{700} - 60$.

Importantly, both the radiosonde and ERA5 data indicate a similiar linear relationship between T_{700} and ε that suggests the entrainment rate increases with lower tropospheric temperatures. The slopes of the ERA5 and radiosonde regression lines are statistically indistinct from each other. The higher y-intercept in the radiosonde data indicates that - at a given lower tropospheric temperature - the radiosonde data are cooler than their ERA5 counterparts (i.e., a higher entrainment rate is required to match upper tropospheric temperatures in the radiosonde data).

The linear relationship between temperature and the entrainment rate is further exemplified in Figs. 3b and 3d. The dots in Fig. 3b show annual-mean 250hPa temperatures plotted as a function of annual-mean 700 hPa temperatures for all years in the CESM output (gray) and observations (black). The lines show 250hPa temperatures predicted by integrating Eq. 3 using an entrainment rate given by the linear fits in Fig. 3a (Eqs. 4a and 4b). The linear fits in Fig. 3a clearly provide a very good estimate of the entrainment rate required to simulate both CESM and observed upper tropospheric temperatures across a range of temperatures. The results in Fig. 3d show analogous results, but use the fits in Fig. 3c to compare results based on RAOB and ERA5 results sampled where RAOB data. In both cases, the linear fits in Fig. 3c provide a good estimate of the entrainment rate required to match observed upper tropospheric temperatures. Note that - as discussed above - at a given 700hPa temperature the radiosonde data are systematically cooler at the 250hPa level than their ERA5 counterparts.

Finally, Figs. 2c and 2f show the complete vertical profiles of ΔT_{ε} derived using the linear fits in Fig. 2b for the range of 700hPa temperatures found in CESM and ERA5. The linear

relationships given in Fig. 4a act to minimize ΔT_ε not only at 250hPa (by construction), but thoughout much of the troposphere.

The amplitudes of the linear relationships between lower tropospheric temperatures and the entrainment rate (as indicated in Fig. 3a) vary depending on details of the analysis design. Nevertheless, they are significantly positive under a range of parameter changes. For examples: Moving the level where ΔT_ε is minimized to 500hPa yields a slope $\frac{\Delta \varepsilon}{\Delta T_{700}}$ of $0.15 \pm 0.00 K^{-1}$ in CESM output - which is similar to that in Fig. 3a - and increases the slope in ERA5 data to $0.34 \pm 0.04\ K^{-1}$. Alternatively, keeping the level where ΔT_ε is minimized at 250hPa but lowering "cloud base" to 850hPa reduces the slopes in both CESM output and ERA5: $\frac{\Delta \varepsilon}{\Delta T_{850}} = 0.06 \pm 0.00 K^{-1}$ in CESM output and $0.05 \pm 0.02\ K^{-1}$ in ERA5.

In summary, the key findings in Figs. 1-3 are that 1) the zero buoyancy plume model is capable of simulating the long term changes in free tropospheric temperatures found in climate change simulations *only* when the entrainment rate increases with temperature; 2) the required increases in the entrainment rate vary linearly with lower tropospheric temperature; and 3) similarly positive relationships between temperatures and the inferred entrainment rate are found in both ERA5 and RAOB data. The positive linear relationships between temperature and the entrainment rate are robust to changes in the analysis procedure. They are reproducible in large ensembles from the three other Earth System Models considered in this study (Appendix Fig. A1). And they are robust to adjusting the entrainment rate to account for the decreasing coverage of convection with height (not shown; see Zhou and Xie 2019 Eq. 2; Bao et al., 2021 Eq. 5). We also checked whether the results might arise from changes in the relative humidity in Eq. 3. Based on the plume model, the changes in relative humidity required to explain the changes in ΔT are roughly 25% over the 1950-2100 period. In contrast, we found the linear trend in tropical-mean relative humidity from CESM to be less than 1% throughout the lower troposphere across the same period (not shown).

5. Implications

The inferred relationship between temperature and the convective entrainment rate has implications for changes in both the mean (Singh and O'Gorman 2013; Seeley and Romps, 2015; Miyawaki et al. 2020) and variance of tropical temperatures under global warming.

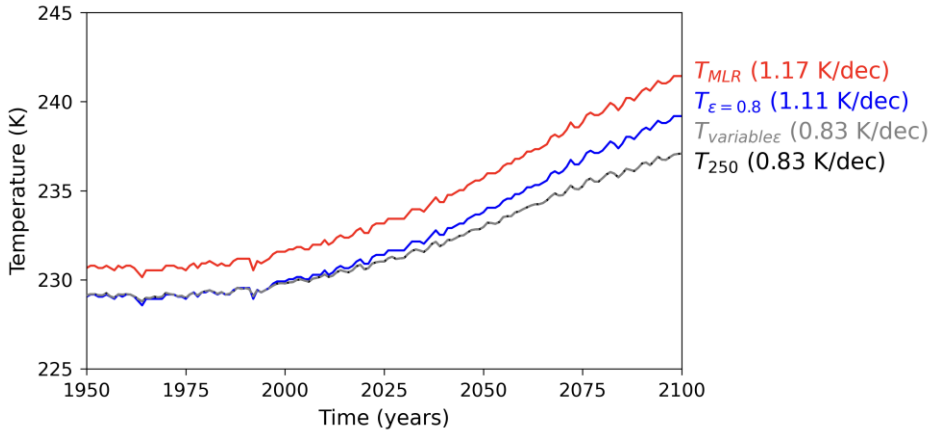

Figure 4. Time series of tropical-mean temperatures at 250 hPa from 1950 to 2100. The black solid line shows tropical-mean 250hPa temperature averaged over all 40 climate change simulations in CESM1. The red solid line indicates the tropical-mean 250hPa temperature predicted by integrating the plume vertically from 700hPa with $\epsilon = 0$ (i.e., equivalent to the moist lapse rate). The blue solid line shows tropical-mean 250hPa temperature predicted by integrating the plume vertically from 700hPa with 8. The gray dashed line shows tropical-mean 250hPa temperature predicted by integrating the plume vertically from 700hPa where the entrainment rate varies as per the fit in Fig. 3a (given in Eq. 4b). Trends are calculated over the period 2050-2100.

Implications for trends in mean tropical temperatures

The implications for tropical-mean temperature trends are summarized in Figure 4. The grey line show the *actual* ensemble-mean 250hPa temperatures averaged over the tropics from the CESM large-ensemble of climate change simulations. Upper tropospheric temperatures increase from ~228 K in 1950 to 237 K in 2100, and the mean warming rate over the latter half of the 21st century is ~0.8 K/decade.

The red line shows temperatures predicted by integrating CESM 700hPa temperatures vertically using the moist lapse rate. Note that this is equivalent to applying the plume model (Eq. 3) with an entrainment rate of $\varepsilon = 0$. In 1950, the 250hPa temperatures predicted by the moist lapse rate (T_{MLR}) are ~231K, or ~2K warmer than those simulated by the model, consistent with the differences between tropical-mean temperatures and a moist adiabat found in the climatological-mean. By 2100, T_{MLR} reaches ~242K, which is roughly ~5K warmer than those simulated by the model. By the last half of the 21st century, the upper tropospheric warming predicted by the moist lapse rate is about 50% larger (~1.2 K/dec vs. 0.8 K/dec) than that indicated by CESM.

The blue line shows temperatures predicted by integrating CESM 700hPa temperatures vertically using the plume model with a fixed entrainment rate of 0.8. As discussed earlier, $\varepsilon = 0.8$ provides a close fit to the tropical-mean lapse rate between 700 and 250hPa in the historical period. Thus 250hPa temperatures predicted by the plume model closely match those simulated by the CESM in 1950 by construction. However, using a fixed entrainment rate leads to a notable overestimate of the long-term warming of the tropical troposphere. In the case of $\varepsilon = 0.8$, the plume model overpredicts the simulated warming rate at 250hPa by ~40% (~1.1 K/dec vs. ~0.8 K/dec) and yields temperatures in 2100 that exceed the actual temperatures by ~2K (~239K vs. 237K).

Finally, the black line shows temperatures predicted by integrating 700hPa temperatures vertically using the plume model with an entrainment rate that varies linearly with temperature as given by Fig. 3a and Eq. 4b. The temperatures at 250hPa that are predicted by applying Eq. 4b to the plume model are indistinguishable from those found in the CESM simulations. The warming rate estimated by the plume model for the case where ε is given by Eq. 4b is effectively identical to the actual warming rate (0.83 K/dec).

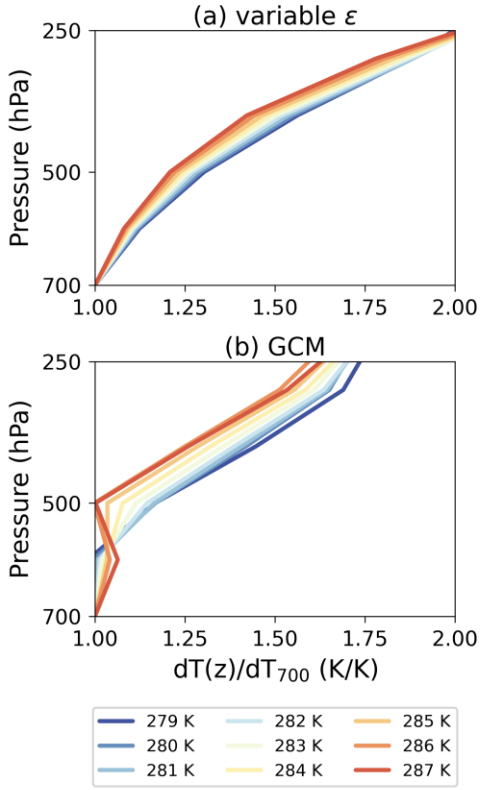

Figure 5. The amplitude of annual-mean tropospheric temperature variability with respect to temperature variability at 700hPa (i.e., $\frac{dT(z)}{dT_{700hPa}}$). Top panels show $\frac{dT(z)}{dT_{700hPa}}$ based on the zero-buoyancy model with a varying entrainment rate determined by the linear fit shown in Fig. 3a. Bottom panels show results based on CESM1 output. The derivative is estimated empirically from annual mean data using a bin size of 0.12 K and 5 K for 700hPa temperatures based on the zero-buoyancy model and the CESM1 output, respectively. Colors indicate the centered value of 700hPa temperature of each bin which the derivatives $\frac{dT(z)}{dT_{700hPa}}$ are calculated. Results are based on the range of 700hPa temperatures found in the CESM1 simulations over the period 1950-2100.

Implications for trends in the variance of tropical temperatures

The implications of the results for changes in tropical-mean temperature *variability* are summarized in Figure 5. The temperature variability at a given height level z with respect to the variability at 700hPa can be expressed as the ratio $\frac{dT(z)}{dT_{700hPa}}$. If the lapse rate between 700hPa and z is fixed, then $\frac{dT(z)}{dT_{700hPa}} = 1$ for all temperatures. But if the lapse varies with temperature, as is the case with the moist lapse rate, then so must $\frac{dT(z)}{dT_{700hPa}}$. Figure 5a shows the ratio $\frac{dT(z)}{dT_{700hPa}}$ calculated from the plume model using the linear expression for the entrainment rate given by Eq. 4b. The line colors indicate different 700hPa temperatures used as a starting point for the lapse rate. The derivatives are estimated for bin sizes of 0.12 K in 700hPa temperatures. By

434 construction, $\frac{dT(z)}{dT_{700hPa}} = 1$ at z=700hPa for all temperatures. We focus on results below 250 hPa
435 where temperatures transition to radiative equilibrium and moist adiabatic processes are less
436 relevant for interpreting the temperature profile (Folkins 2002; Keil et al. 2019). As lower
437 tropospheric temperatures increase, the ratio $\frac{dT(z)}{dT_{700hPa}}$ derived from the model decreases
438 throughout the tropical troposphere up to 250hPa (Fig. 5a). In the middle troposphere, $\frac{dT(z)}{dT_{700hPa}}$
439 decreases from ~1.5 to ~1.35, or about ~10%.

440 Figure 5b shows $\frac{dT(z)}{dT_{700hPa}}$ calculated from the CESM climate change simulations, where
441 the derivative is estimated using a wider bin size of 5 K (i.e., $T_{700hPa} \pm 2.5\ K$) to reduce the
442 sampling errors that may arise from the large internal variability. The different bin size within a
443 range of 0.3-8 K does not qualitatively affect the results of the regressions (not shown). Results
444 are calculated for all annual-temperature profiles in all 40 year simulations and across all
445 ensemble members. In the mid-upper troposphere above ~600hPa, the CESM climate change
446 output generally yields decreases in $\frac{dT(z)}{dT_{700hPa}}$ reminiscent of those predicted by the plume model,
447 albeit there is some scatter in the results for individual temperature lines.

448 Why do changes in $\frac{dT(z)}{dT_{700hPa}}$ matter? The ratio indicates how upper tropospheric
449 temperatures vary per unit change in lower tropospheric temperature. It thus provides a measure
450 of how the vertical structure of internal tropical tropospheric variability might change under
451 global warming. For example, consider the case of ENSO variability. Decreases in $\frac{dT(z)}{dT_{700hPa}}$
452 suggest that the same ampitude ENSO event in surface temperature will have a weaker
453 projection onto upper tropical tropospheric temperatures and - potentially - the ensuing
454 teleconnections. We defer analysis of the implications of the results in Fig. 5 for changes in
455 internal climate variability under global warming to a companion study.
456
457 **6. Discussion**
458 The vertical profile of tropical-mean temperatures exhibits well-known departures from a
459 moist adiabat. Upper tropical tropospheric temperatures are several degrees less than those
460 predicted by a moist adiabat in the climatological-mean (Singh and O'Gorman 2013; Keil et al.,
461 2019; Po-Chedley et al. 2019; Keil et al., 2019; Miyawaki et al. 2020). The tropical troposphere

462 warms less than that predicted by a moist adiabat in observations (e.g., Santer et al. 2005; Steiner
463 et al. 2020) and climate change simulations (e.g., Santer et al. 2005; Romps and Kuang 2010;
464 Romps 2011; Muller et al. 2011; Sobel and Camargo 2011; Fasullo 2012; Singh and O'Gorman
465 2013; Seeley and Romps, 2015; Zhou and Xie, 2019; Miyawaki et al. 2020; Bao and Stevens
466 2021; Bao et al. 2021).

467 The climatological-mean differences between tropical-mean temperatures and those
468 predicted by a moist adiabat (ΔT) are thought to arise from a variety of factors, including the
469 entrainment of environmental air into convecting plumes, the fact that the tropical-mean reflects
470 an average over plumes at a range of different heights, and the effects of the large-scale
471 circulation (Singh and O'Gorman, 2013; Zhou and Xie, 2019; Keil et al., 2019; Miyawaki et al.,
472 2020; Bao and Stevens, 2021). The increases in ΔT under climate change have been primarily
473 linked to increases in the saturation vapor deficit of the environment $q_e^* - q_e$, which increases
474 the efficiency of convective entrainment since the mixing between convective plumes and the
475 environment is acting on larger gradients in moist static energy (Singh and O'Gorman 2013;
476 Seeley and Romps 2015).

477 Here we have used the zero-buoyancy plume model of Singh and O'Gorman (2013) to
478 provide novel insights into the factors that govern the increases in ΔT - and thus in CAPE - under
479 climate change. The key findings are the following:

480 1) The increases in ΔT under climate change are only partially explained by increases in
481 the saturation vapor deficit in the plume model. Rather, the increases in ΔT are only simulated
482 when the entrainment rate ε that acts on the saturation vapor deficit also increases with
483 temperature.

484 2) The required increases in ε exhibit a robust linear relationship with lower-tropospheric
485 (i.e., cloud base) temperature. Simulations based on the plume model indicate that the
486 entrainment rate required to reproduce the upper tropospheric warming in climate change
487 simulations roughly doubles over the 21st century.

488 3) The linear relationship between lower tropospheric temperature and the entrainment
489 rate ε emerges in both climate change simulations and observations based on ERA5 and
490 radiosonde measurements. The amplitude of the linear relationship varies depending on details of
491 the analysis. But the sign and robustness of the linear relationship is reproducible when the cloud
492 base level is lowered to 850hPa, when the level used to fit the plume model to actual

temperatures is lowered from 250hPa to 500hPa, and in large ensembles of climate change simulations run on different ESMs. The results can not be explained by realistic changes in the environmental relative humidity of the plume model.

4) The results have implications for understanding long-term trends in tropical-mean temperatures. The warming rate of the upper tropical troposphere in climate change simulations run on CESM1 with RCP8.5 forcings is roughly 0.8 K/dec. In contrast, the warming rate of the upper tropical troposphere predicted by integrating CESM1 lower-tropospheric temperatures vertically using the plume model is (a) ~1.2 K/dec if free-tropospheric temperatures are determined from a moist adiabat (i.e., $\varepsilon = 0$); and (b) ~1.1 K/dec if free-tropospheric temperatures are determined from the plume model run with a fixed entrainment rate ($\varepsilon = 0.8$) acting on increases in the saturation vapor deficit. The warming rate of the upper tropical troposphere found in the CESM climate change simulations is *only* recovered when the plume model is run with an entrainment rate that roughly doubles over the course of the simulation. A similar relationship between the overprediction of tropical tropospheric warming and the entrainment rate was highlighted in Miyawaki et al. (2020), but their analysis focused on the effects of a fixed value of ε on trends in ΔT; they did not consider time-varying changes in ε as a function of lower tropospheric temperatures.

5) The results also have implications for changes in the variance of tropical-mean temperatures. The plume model predicts a roughly 5% decrease in the ratio of upper to lower tropical temperature variance for a warming of 4K. Qualitatively similar changes in variance are found in the ESMs over the course of the 21st century.

The changes in the entrainment rate indicated here could arise from a range of physical processes, including changes in the amplitude of turbulent mixing associated with individual convective plumes and/or variations in the depth and strength of convective plumes across the tropics (Xu et al., 2021; Bao et al., 2021; Sarve 2022). It remains to be determined which of these processes are key for the inferred increases in the entrainment rate with climate change indicated here.

Acknowledgments: D.W.J.T. and S.Y. are supported by the NSF Climate and Large-Scale Dynamics program. The CESM project is supported primarily by the U.S. National Science Foundation. The authors acknowledge the Climate Simulation Laboratory at NCAR's

Computational and Information Systems Laboratory (CISL; sponsored by NSF and other agencies) and the MIT's Massachusetts Green High Performance Computing Center (supported by the Center for Sustainability Science and Strategy) for providing computing and storage resources. We thank Paul O'Gorman and Benjamin D. Santer for their helpful comments on the manuscript.

Availability Statement: All climate model datasets used in this study are publicly available via the NCAR Multi-Model Large Ensemble Archive (MMLEA) at https://www.cesm.ucar.edu/community-projects/mmlea as cited in Deser et al. (2020).

Appendix

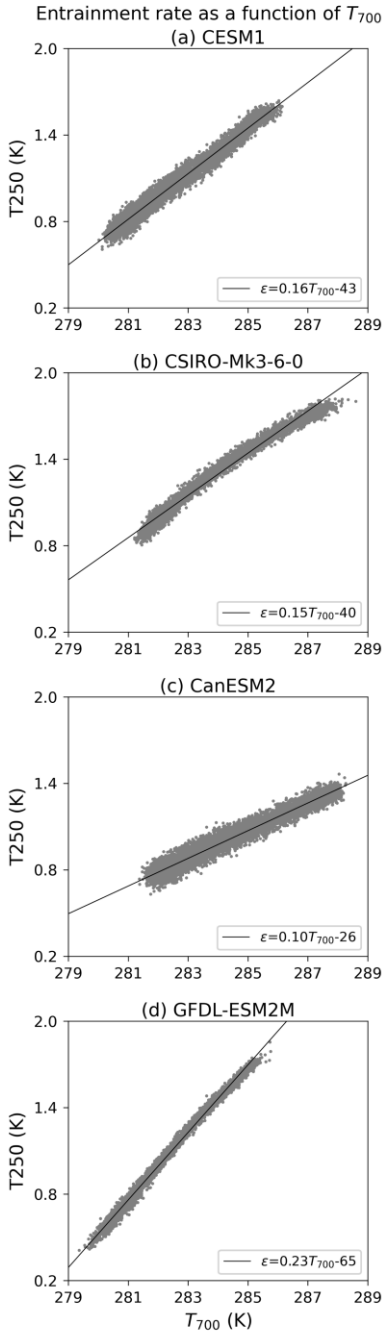

Figure A1. As in the grey dots in Fig. 3a, but for the ESMs other than CESM listed in Section 2. Slopes are given on the panels.

References

Bao, J., and B. Stevens, 2021: The elements of the thermodynamic structure of the tropical atmosphere. Journal of the Meteorological Society of Japan. Ser. II, 99, 1483-1499.

542 Bao, J., B. Stevens, L. Kluft, and D. Jiménez-de-la-Cuesta, 2021: Changes in the tropical lapse
543 rate due to entrainment and their impact on climate sensitivity. Geophysical Research Letters,
544 48, e2021GL094969.
545 Charney, J. G., 1963: A note on large-scale motions in the tropics. Journal of Atmospheric
546 Sciences, 20, 607-609.
547 Chen, J., and A. Dai, 2023: The atmosphere has become increasingly unstable during 1979–2020
548 over the Northern Hemisphere. Geophysical Research Letters, 50, e2023GL106125.
549 ——, 2023: The atmosphere has become increasingly unstable during 1979–2020 over the
550 Northern Hemisphere. Geophysical Research Letters, 50, e2023GL106125.
551 Deser, C., and Coauthors, 2020: Insights from Earth system model initial-condition large
552 ensembles and future prospects. Nature Climate Change, 10, 277-286.
553 Durre, I., X. Yin, R. S. Vose, S. Applequist, and J. Arnfield, 2018: Enhancing the data coverage
554 in the integrated global radiosonde archive. Journal of Atmospheric and Oceanic Technology,
555 35, 1753-1770.
556 Fasullo, J., 2012: A mechanism for land–ocean contrasts in global monsoon trends in a warming
557 climate. Climate Dynamics, 39, 1137-1147.
558 Flannaghan, T. J., S. Fueglistaler, I. M. Held, S. Po-Chedley, B. Wyman, and M. Zhao, 2014:
559 Tropical temperature trends in atmospheric general circulation model simulations and the
560 impact of uncertainties in observed SSTs. Journal of Geophysical Research: Atmospheres, 119,
561 13,327-313,337.
562 Folkins, I., 2002: Origin of lapse rate changes in the upper tropical troposphere. Journal of the
563 atmospheric sciences, 59, 992-1005.
564 Gettelman, A., D. Seidel, M. Wheeler, and R. Ross, 2002: Multidecadal trends in tropical
565 convective available potential energy. Journal of Geophysical Research: Atmospheres, 107,
566 ACL 17-11-ACL 17-18.
567 Hersbach, H., and Coauthors, 2020: The ERA5 global reanalysis. Quarterly journal of the royal
568 meteorological society, 146, 1999-2049.
569 Hurrell, J. W., and Coauthors, 2013: The community earth system model: a framework for
570 collaborative research. Bulletin of the American Meteorological Society, 94, 1339-1360.

571 Jeffrey, S., and Coauthors, 2013: Australia's CMIP5 submission usingthe CSIRO-Mk3. 6 model.
572 Australian Meteorological and Oceanographic Journal, 63, 1-13.
573 Kay, J. E., and Coauthors, 2015: The Community Earth System Model (CESM) large ensemble
574 project: A community resource for studying climate change in the presence of internal climate
575 variability. Bulletin of the American Meteorological Society, 96, 1333-1349.
576 Keil, P., H. Schmidt, B. Stevens, and J. Bao, 2021: Variations of tropical lapse rates in climate
577 models and their implications for upper-tropospheric warming. Journal of Climate, 34, 9747-
578 9761.
579 Kirchmeier-Young, M. C., F. W. Zwiers, and N. P. Gillett, 2017: Attribution of extreme events in
580 Arctic sea ice extent. Journal of Climate, 30, 553-571.
581 Lawson, R., 1990: Thermodynamic analyses of buoyancy and entrainment in cumuli using
582 measurements from a radiometric thermometer. 1990 Conference on Cloud Physics, San
583 Francisco, CA, 685-692.
584 Miyawaki, O., Z. Tan, T. A. Shaw, and M. F. Jansen, 2020: Quantifying key mechanisms that
585 contribute to the deviation of the tropical warming profile from a moist adiabat. Geophysical
586 Research Letters, 47, e2020GL089136.
587 Muller, C. J., P. A. O'Gorman, and L. E. Back, 2011: Intensification of precipitation extremes with
588 warming in a cloud-resolving model. Journal of Climate, 24, 2784-2800.
589 Po- Chedley, S., M. D. Zelinka, N. Jeevanjee, T. J. Thorsen, and B. D. Santer, 2019: Climatology
590 explains intermodel spread in tropical upper tropospheric cloud and relative humidity response
591 to greenhouse warming. Geophysical Research Letters, 46, 13399-13409.
592 Riemann-Campe, K., K. Fraedrich, and F. Lunkeit, 2009: Global climatology of convective
593 available potential energy (CAPE) and convective inhibition (CIN) in ERA-40 reanalysis.
594 Atmospheric Research, 93, 534-545.
595 Rodgers, K. B., J. Lin, and T. L. Frölicher, 2015: Emergence of multiple ocean ecosystem drivers
596 in a large ensemble suite with an Earth system model. Biogeosciences, 12, 3301-3320.
597 Romps, D. M., 2011: Response of tropical precipitation to global warming. Journal of the
598 Atmospheric Sciences, 68, 123-138.
599 Romps, D. M., and A. B. Charn, 2015: Sticky thermals: Evidence for a dominant balance between
600 buoyancy and drag in cloud updrafts. Journal of the Atmospheric Sciences, 72, 2890-2901.

Romps, D. M., and Z. Kuang, 2010: Do undiluted convective plumes exist in the upper tropical troposphere? Journal of the Atmospheric Sciences, 67, 468-484.

Romps, D. M., J. T. Seeley, D. Vollaro, and J. Molinari, 2014: Projected increase in lightning strikes in the United States due to global warming. Science, 346, 851-854.

Santer, B. D., and Coauthors, 2017: Comparing tropospheric warming in climate models and satellite data. Journal of Climate, 30, 373-392.

Santer, B. D., and Coauthors, 2005: Amplification of surface temperature trends and variability in the tropical atmosphere. Science, 309, 1551-1556.

Savre, J., 2022: What controls local entrainment and detrainment rates in simulated shallow convection? Journal of the Atmospheric Sciences, 79, 3065-3082.

Seeley, J. T., and D. M. Romps, 2015: Why does tropical convective available potential energy (CAPE) increase with warming? Geophysical Research Letters, 42, 10,429-410,437.

Sherwood, S. C., D. Hernández-Deckers, M. Colin, and F. Robinson, 2013: Slippery thermals and the cumulus entrainment paradox. Journal of the Atmospheric Sciences, 70, 2426-2442.

Singh, M. S., and P. A. O'Gorman, 2013: Influence of entrainment on the thermal stratification in simulations of radiative-convective equilibrium. Geophysical Research Letters, 40, 4398-4403.

Sobel, A. H., and C. S. Bretherton, 2000: Modeling tropical precipitation in a single column. Journal of climate, 13, 4378-4392.

Sobel, A. H., and S. J. Camargo, 2011: Projected future seasonal changes in tropical summer climate. Journal of Climate, 24, 473-487.

Soden, B. J., and I. M. Held, 2006: An assessment of climate feedbacks in coupled ocean–atmosphere models. Journal of climate, 19, 3354-3360.

Soden, B. J., D. L. Jackson, V. Ramaswamy, M. Schwarzkopf, and X. Huang, 2005: The radiative signature of upper tropospheric moistening. Science, 310, 841-844.

Soden, B. J., R. T. Wetherald, G. L. Stenchikov, and A. Robock, 2002: Global cooling after the eruption of Mount Pinatubo: A test of climate feedback by water vapor. science, 296, 727-730.

Steiner, A. K., and Coauthors, 2020: Observed temperature changes in the troposphere and stratosphere from 1979 to 2018. Journal of Climate, 33, 8165-8194.

Stone, P. H., and J. H. Carlson, 1979: Atmospheric lapse rate regimes and their parameterization. Journal of Atmospheric Sciences, 36, 415-423.

Taszarek, M., J. T. Allen, M. Marchio, and H. E. Brooks, 2021: Global climatology and trends in convective environments from ERA5 and rawinsonde data. NPJ climate and atmospheric science, 4, 35.

Wei, D., A. M. Blyth, and D. J. Raymond, 1998: Buoyancy of convective clouds in TOGA COARE. Journal of the atmospheric sciences, 55, 3381-3391.

Xu, X., C. Sun, C. Lu, Y. Liu, G. J. Zhang, and Q. Chen, 2021: Factors affecting entrainment rate in deep convective clouds and parameterizations. Journal of Geophysical Research: Atmospheres, 126, e2021JD034881.

Zhou, W., and S.-P. Xie, 2019: A conceptual spectral plume model for understanding tropical temperature profile and convective updraft velocities. Journal of the Atmospheric Sciences, 76, 2801-2814.